Pure Appl. Chem., Vol. 82, No. 6, pp. 1317–1327, 2010.
doi:10.1351/PAC-CON-09-10-23

Liquid-phase laser ablation*

Koichi Sasaki[1,‡] and Noriharu Takada[2]

[1]Division of Quantum Science and Engineering, Hokkaido University, Sapporo 060-0828, Japan; [2]Department of Electrical Engineering and Computer Science, Nagoya University, Nagoya 464-8603, Japan

Abstract: The irradiation of an intense laser pulse onto a solid target immersed in liquid produces dense plasma. The plasma produced by liquid-phase laser ablation has unique features at high pressure and temperature, which are never realized by liquid-phase discharges. Another unique characteristic of liquid-phase laser ablation is the formation of a cavitation bubble. This article reports the fundamental aspects of liquid-phase laser-ablation plasmas, cavitation bubbles, and the formation processes of nanoparticles, together with some applications of liquid-phase laser ablation.

Keywords: cavitation bubble; high pressure; laser ablation; liquid phase; nanoparticles.

INTRODUCTION

Recently, liquid-phase discharge attracts much attention as a new subject in the research field of reactive plasmas [1]. Laser ablation is an alternative method for producing plasmas in liquids. The electrical discharges in liquids would have difficulty in the way of power deposition. In the case of laser ablation, it is very easy to produce plasmas in liquids since just focusing intense laser beams onto solid-state targets immersed in liquids is sufficient, provided that the liquid is transparent at the laser wavelength.

The history of laser-ablation research is more or less similar to that of reactive plasmas. Researchers in the field of laser processing have studied laser ablation in vacuum and in ambient gases for a long time. The applications of gas-phase laser ablation to material syntheses are formation of thin films (pulsed laser deposition; PLD) and production of nanoparticles. Recently, some research, including the author's, noticed the importance of liquid-phase laser ablation, and shifted their interest to this new subject [2–10]. When the research of liquid-phase laser ablation started, the advantages from technical viewpoints were emphasized. The technical advantages of liquid-phase laser ablation are the low cost because of the absence of vacuum equipment and the easy collection of nanoparticles after the synthesis. The latter advantage is due to the fact that nanoparticles are stored in the liquid as a colloidal solution in liquid-phase laser ablation.

The authors are currently interested in unusual features of liquid-phase laser ablation rather than the technical advantages. The expansion of particles ejected from the target is restricted significantly in liquid-phase laser ablation because of the tight confinement effect of the ambient liquid. The restricted expansion results in high pressure and temperature of the plasma. Another unusual feature is the formation of a cavitation bubble after the disappearance of plasma with optical emission. These unusual features are never realized by liquid-phase discharges. In this article, we report fundamental aspects of liquid-phase laser ablation, together with some examples of its applications.

---

*Paper based on a presentation at the 19th International Symposium on Plasma Chemistry (ISPC-19), 26–31 July 2009, Bochum, Germany. Other presentations are published in this issue, pp. 1189–1351.

‡Corresponding author

ESTIMATIONS OF PLASMA PRESSURE AND TEMPERATURE

We installed a graphite target in distilled water, and irradiated it with an Nd:YAG laser pulse at a wavelength of 1.06 μm. The duration of the YAG laser pulse was 10 ns, and the fluence on the target surface was 28 J/cm^2. We took the photograph of the optical emission intensity from the plasma using a charge-coupled device (ICCD) camera with a gated image intensifier. The gate width was 2 ns. Figure 1 shows the temporal variations of the maximum intensity and the plasma size in the optical emission image [11]. The spatial distribution of the optical emission intensity had a smooth shape (see Fig. 10a), and we found no distinct boundaries between the plasma with optical emission and the water phase. The plasma size shown in Fig. 1 is defined as the full width at half maximum in the parallel direction to the target surface. The pulse shape of the optical emission intensity shown in Fig. 1 is quite similar to the waveform of the YAG laser pulse. The plasma size expanded rapidly from 0 to 10 ns at an expansion speed of 2.4×10^7 mm/s. The plasma continued the expansion after 10 ns at a slower expansion speed of 5×10^6 mm/s. These expansion speeds were slower than those observed in gas-phase laser ablation, where the expansion speed of a plume is on the order of 10^8 mm/s. The slower expansion speed in liquid-phase laser ablation is attributed to the tight confinement effect of ambient water.

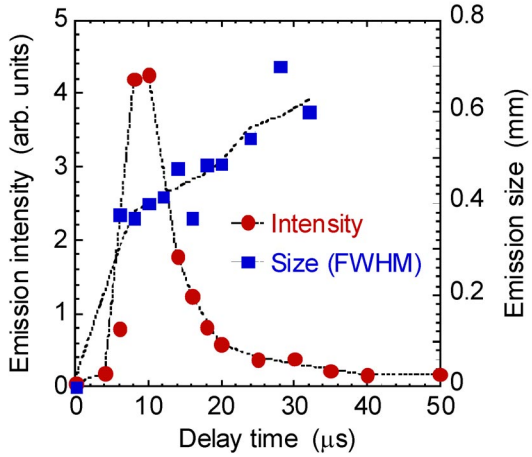

Fig. 1 Temporal variation of the maximum optical emission intensity and the emission size observed when a graphite target immersed in water was irradiated by a YAG laser pulse at 1.06 μm.

Figure 2 shows optical emission spectra observed from the plasma [11]. The gate of the ICCD camera connected to a spectrograph was opened for 50 ns at various delay times after laser ablation. The wavelength dependence of the sensitivity of the spectrograph including the ICCD camera was calibrated using a tungsten standard lamp. As shown in Fig. 2, we observed continuum spectra with no line emissions. This may be because the plasma is so dense that it is seen as a black body from the outside. The black body temperature was evaluated by fitting the continuum spectra with the Planck equation. As a result, as indicated in Fig. 2, the black body temperature at 0–50 ns was as high as 4300 K. The black body temperature decreased with time, and was 2500 K at 1 μs after laser ablation.

We roughly estimated the pressure of the plasma from the number of particles ejected from the target [12]. When we used a Ti target immersed in water, the total number of Ti atoms ejected from the target by the irradiation of a laser pulse was estimated to be 1×10^{15} from the volume of the crater formed on the target surface. Based on this number, the plasma size, and the black body temperature, the pressure of the plasma at 4 ns after the irradiation of the YAG laser pulse was evaluated to be 0.8 GPa. Another way for estimating the plasma pressure was to use an equation reported in [13], where

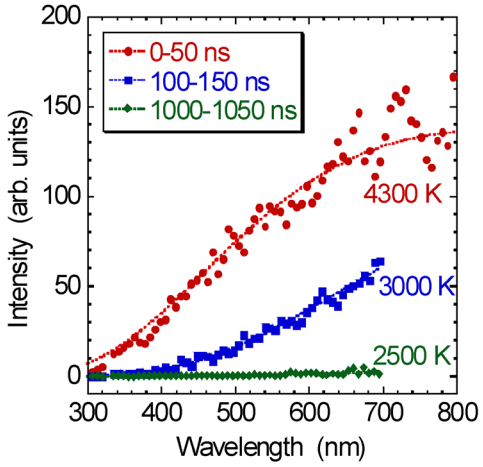

Fig. 2 Optical emission spectra observed from a laser-ablation graphite plasma produced in water. The temperatures were evaluated by fitting the spectra with the Planck equation.

the authors estimated the plasma pressure from the pressure of the shock wave. According to the equation, the plasma pressure was estimated to be 1 GPa at the experimental condition. Accordingly, it is considered that the laser-ablation plasma produced in water has a high pressure of 10^4 atm, which is never realized by discharges.

DYNAMICS OF CAVITATION BUBBLE

The experimental apparatus for observing cavitation bubbles by shadowgraph imaging is shown in Fig. 3. A Ti target was installed in a small vessel which was filled with distilled water. The target was irradiated by Nd:YAG laser pulses from the normal direction. The duration and the energy of the laser pulse were 10 ns and 22 mJ, respectively. The radius of the laser beam on the target surface was estimated to be 0.2 mm from the radius of the crater formed on the target. The vessel had view ports. The ablation space was illuminated by flash lamp light, and the image of the transmitted lamp light was

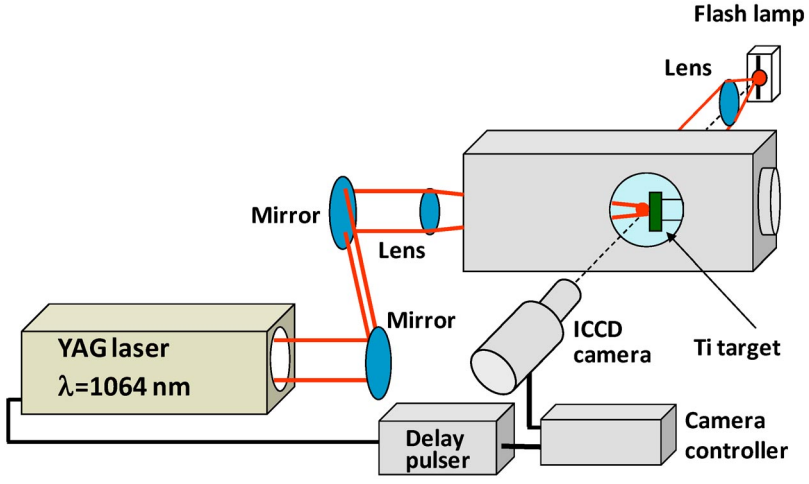

Fig. 3 Experimental apparatus for shadowgraph imaging in liquid-phase laser ablation.

captured using an ICCD camera. By changing the delay time between the oscillation of the YAG laser and the gate of the ICCD camera, we obtained the snapshots of cavitation bubbles at various delay times after laser ablation. The gate width of the ICCD camera was 50 ns.

Figure 4 shows shadowgraph images observed at various delay times after the irradiation of the YAG laser pulse [14]. The shadowgraph image shown in Fig. 4a, which was observed at 0.7 μs after laser ablation, represents the propagation of a spherical shock wave originated from the ablation point. The propagation speed of the wave agreed well with the sound velocity in water. Figure 4a also shows the birth of a cavitation bubble, which may be induced by abrupt vaporization of water due to the production of plasma with high temperature and pressure. The cavitation bubble expanded with time. We observed an interesting phenomenon shown in Fig. 4b at a delay time of 26 μs [15]. The picture shown in Fig. 4b suggests the ejection of child bubbles from the main cavitation bubble. The maximum bubble size was observed at 90 μs as shown in Fig. 4c. After the maximum size, the cavitation bubble shrunk with time. The generation of the second shock wave, which was induced by the collapse of the cavitation bubble, was observed at around 186 μs as shown in Fig. 4d. The generation of the shock wave suggests the high-temperature, high-pressure state at the collapse of the cavitation bubble. However, no optical emission was observed at the collapse of the cavitation bubble. The generation of the second shock wave was followed by the formation of the second cavitation bubble as shown in Fig. 4e. The shape of a bubble at a long delay time (>250 μs) was not hemispherical, and the expansion and the shrink of the bubble were irregular. The final shape of the bubble was a complete sphere as shown in Fig. 4f, which was observed at 2.4 ms. After the completely spherical bubble was realized, it was observed stationarily in front of the target.

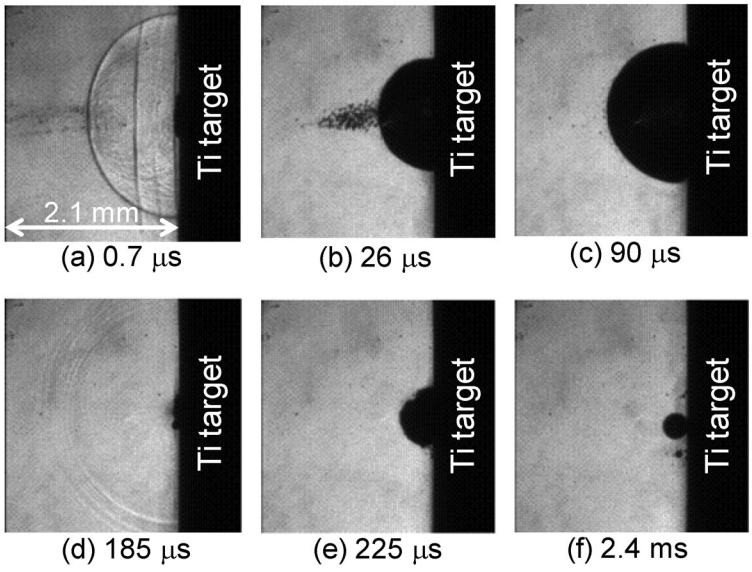

Fig. 4 Snapshots of cavitation bubbles observed at various delay times after laser ablation of a Ti target in water.

The temporal variation of the radius of the cavitation bubble is shown in Fig. 5. The dynamics of a cavitation bubble produced by laser-induced breakdown of water without placing targets is analyzed widely using the Rayleigh–Plesset equation [16]. However, it was found that the agreement between the experimental result and the solution of the conventional Rayleigh–Plesset equation was insufficient in the case of laser ablation with the target. We modified the Rayleigh–Plesset equation by including the contact angle among the target (solid), the water (liquid), and the cavitation bubble (gas), and succeeded

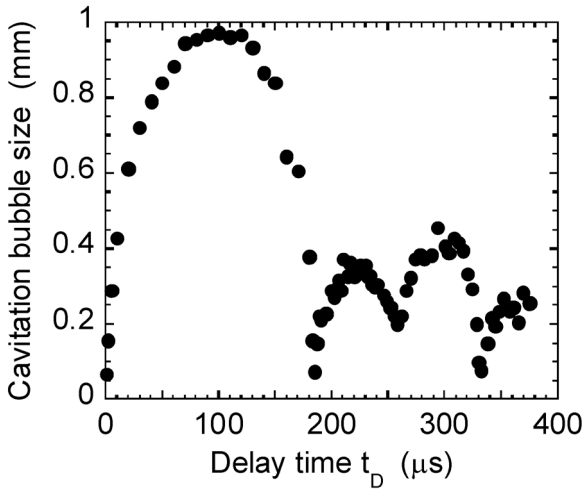

Fig. 5 Temporal variation of the size of the cavitation bubble.

in reproducing the temporal variation of the bubble size shown in Fig. 5 theoretically [17]. The theoretical analysis was used for estimating the pressure and the temperature of the cavitation bubble. It was estimated that the bubble pressure was roughly 16 Torr in the expansion and shrink phases. The bubble pressure was estimated to increase like an impulse to 10 GPa at the collapse. The bubble temperature was estimated to be less than 10 K in the expansion and shrink phases. It increased like an impulse to 10^4 K at the collapse. The details of the theoretical analysis using the modified Rayleigh–Plesset equation will be reported elsewhere.

GROWTH DYNAMICS OF NANOPARTICLES

The first event in liquid-phase laser ablation is the ejection of particles from the target. The ejection of particles is followed by the formation of a cavitation bubble. Therefore, it is pretty sure that ejected particles are located outside of the cavitation bubble in the very early phase. Here is a simple question about the place of the growth of nanoparticles: the inside or the outside of the cavitation bubble. In addition, if nanoparticles are stored inside the cavitation bubble, there is a possibility that nanoparticles are in the high-pressure, high-temperature reaction field at the collapse. To answer these questions, we carried out in situ detection of nanoparticles by laser light scattering [18,19].

The experimental apparatus was similar to Fig. 3, but we injected a pulsed laser beam at 500 nm from the bottom window of the vessel. The image of the scattered laser light was captured using the same ICCD camera that was used for the shadowgraph imaging. The shadowgraph imaging gave us the location and the size of the cavitation bubble, while the location of nanoparticles was known from the image of the scattered laser light. This experimental geometry had an unavoidable problem in the uniform illumination of the laser beam at 500 nm. This was due to the refraction of the laser beam at the boundary between water and the cavitation bubble. It is noted that the laser beam at 500 nm is injected from the bottom of the pictures shown in Fig. 6, and the laser intensity in the upper left part of the cavitation bubble is expected to be weaker than that in the other part. It was confirmed experimentally that the refracted laser beam did not reach the ICCD camera directly.

Figure 6 shows the pictures obtained by illuminating the ablation space by both the flash lamp and the laser beam at 500 nm. As shown in Fig. 6a, which was obtained at 7 μs after laser ablation, we observed the scattered laser light inside the cavitation bubble. This experimental result indicates that the particles ejected from the target are transported toward the cavitation bubble, and the growth of nanoparticles occurs inside the cavitation bubble. The strong scattered laser light was observed in the

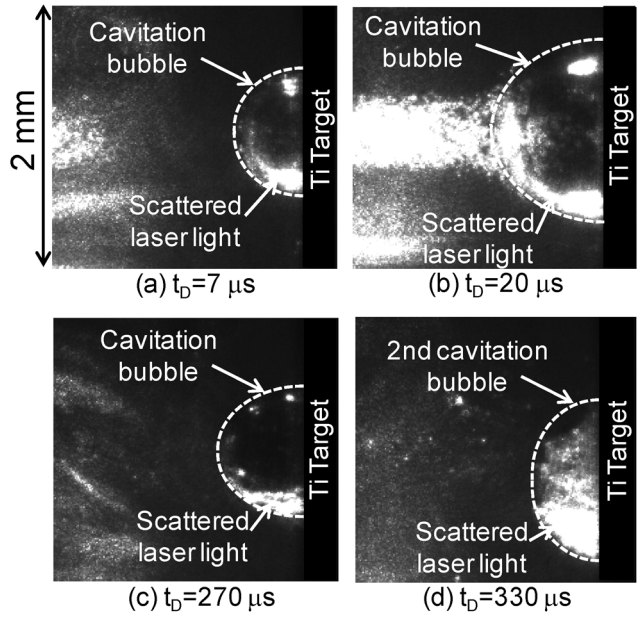

Fig. 6 Snapshots of scattered laser light observed at various delay times after laser ablation, together with the location of the cavitation bubble.

region close to the boundary between water and the cavitation bubble except for the upper left part, suggesting the fast growth of nanoparticles after the transportation into the cavitation bubble. In fact, we detected scattered laser light at a delay time of 0.2 μs after laser ablation. The growth of nanoparticles within 0.2 μs is much faster than the growth of nanoparticles in gas-phase laser ablation. The fast growth may be attributed partly to the low temperature inside the cavitation bubble.

We observed an interesting phenomenon shown in Fig. 6b at a delay time of 20 μs after laser ablation. This experimental result corresponds to the ejection of child bubbles shown in Fig. 4b. It was understood by laser light scattering that the inside of child bubbles shown in Fig. 4b was occupied by nanoparticles. This means the transport of nanoparticles from the cavitation bubble to the water phase. The ejection of nanoparticles was observed at specific delay times, which were dependent on the laser fluence.

In the experimental condition used in Fig. 6, the maximum size of the cavitation bubble was observed at 140 μs after laser ablation, and the collapse of the cavitation bubble was observed at around 280 μs. Figure 6c was observed at a delay time of 270 μs. As shown in Fig. 6c, we observed the scattered laser light from the inside of the cavitation bubble just before the collapse. In other words, a great portion of nanoparticles was stored in the cavitation bubble in the shrink phase, and they were in the high-pressure, high-temperature reaction field at the collapse. Figure 6d shows a picture observed at 330 μs. The bubble was the second cavitation bubble induced by the collapse of the first cavitation bubble. As shown in Fig. 6d, the inside of the second cavitation bubble was occupied by a large amount of nanoparticles. The size and the structure of nanoparticles stored in the cavitation bubble until the collapse would be possibly different from those of nanoparticles ejected from the cavitation bubble in the expansion phase. Further investigation is necessary to understand the relationship between the dynamics of the cavitation bubble and the synthesis characteristics of nanoparticles.

APPLICATION OF LIQUID-PHASE LASER ABLATION

We easily obtain a colloidal solution that includes nanoparticles by ablating a solid-state target immersed in water. To give an example, Fig. 7a shows a picture of a colloidal solution of Au nanoparticles, which was obtained by ablating a Au target immersed in distilled water. Figure 7b shows absorption spectrum of the colloidal solution shown in Fig. 7a. The strong peak at 520 nm corresponds to the absorption due to the surface plasmon of Au nanoparticles. As shown in Fig. 7, laser ablation of a noble metal target produces nanoparticles of the target material. On the other hand, when we use a transition-metal target, we obtain nanoparticles of the transition-metal oxide, indicating strong oxidation property of laser ablation in water.

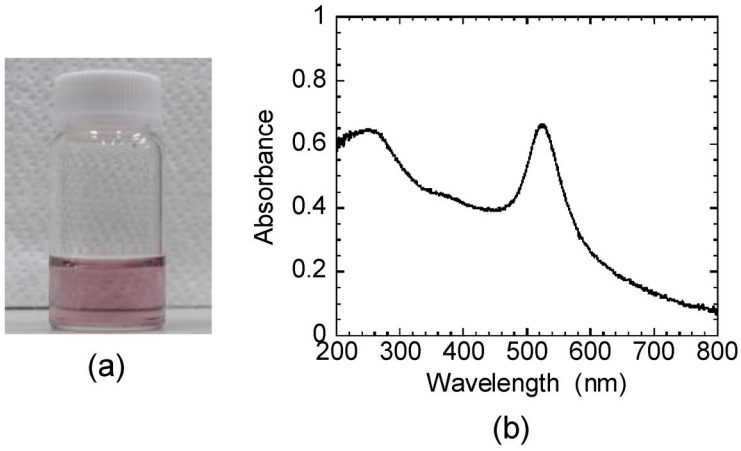

Fig. 7 (a) Picture of colloidal solution of Au nanoparticles and (b) absorption spectrum of the colloidal solution shown in (a).

In this paper, we introduce our unique experiments for synthesizing unoxidized nanoparticles of Ti and Si. The method was laser ablation in liquid N_2 [20]. Ultrahigh-vacuum (UHV) equipment is necessary for synthesizing unoxidized nanoparticles of transition metals by gas-phase laser ablation since oxidation reactions are very efficient. To use liquid N_2 as the medium of laser ablation is an economical way to obtain O_2-free environment. We prepared a stainless-steel chamber with a doubled structure, like a vacuum bottle. The inside of the inner chamber of the doubled structure was filled with liquid N_2, and the space sandwiched by the inner and outer chambers was evacuated using a turbomolecular pump. The evacuation was necessary for the thermal isolation. In addition, in order to prevent the dissolution of O_2 into liquid N_2, the space above the liquid N_2 was purged by pure N_2 gas. YAG laser pulses at the fundamental wavelength of 1.06 μm irradiated Ti and Si targets immersed in liquid N_2. Particles remained in the inner chamber were collected carefully after natural evaporation of liquid N_2.

Figure 8a shows a scanning electron microscopy (SEM) picture and the energy-dispersive spectrometry (EDS) analysis of a nanoparticle produced by laser ablation of a Ti target in liquid N_2. The shapes of nanoparticles were spherical, and the sizes distributed from several micrometers to several tens of nanometers. The atomic ratio of N/Ti along the horizontal line in the SEM picture was approximately 0.4, and the fractional abundance of O was much lower than that of N. These results indicate the production of TiN particles with negligible post-oxidation after the exposure to air. However, it does not deny the existence of very thin oxidized layer on the real surface of the nanoparticle, since the EDS analysis is sensitive not only to the surface but also to the inner body of the nanoparticle. Figure 8b shows a TEM picture and the electron diffraction pattern of nanoparticles. It was understood from the electron diffraction pattern that nanoparticles had a polycrystalline structure of TiN including

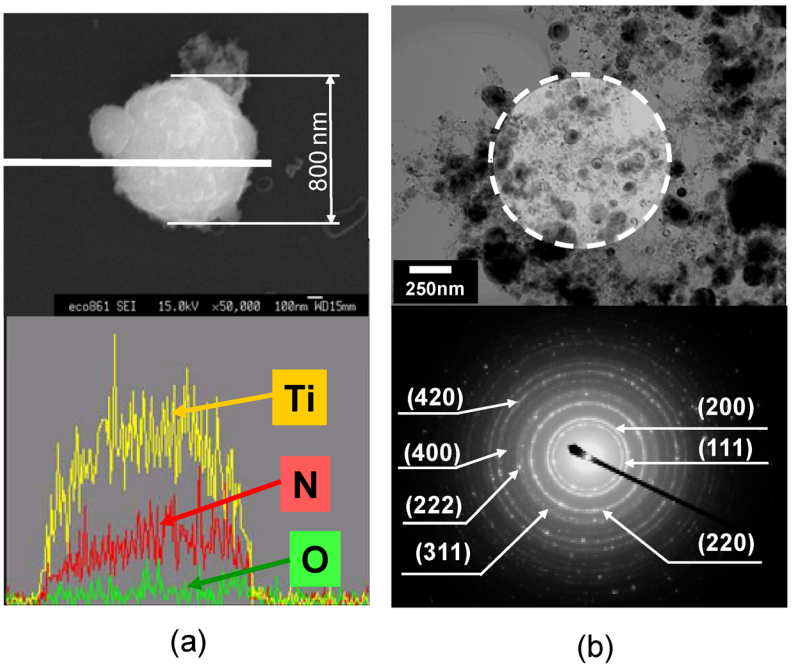

Fig. 8 (a) SEM picture and EDS signal of a nanoparticle produced by laser ablation of a Ti target in liquid N_2. (b) TEM image and the corresponding electron diffraction pattern of nanoparticles produced by laser ablation of a Ti target in liquid N_2.

(200), (111), (220), (311), (222), (400), and (420) orientations. No metallic Ti nanoparticles with crystalline structures were found in the XRD spectrum of nanoparticles. Accordingly, we can say that laser ablation in liquid N_2 is a useful method for synthesizing crystalline TiN particles without using UHV apparatus. In addition, we found a nitrided layer on the surface of the Ti target after the experiment [21]. A distinctive feature of the surface nitriding was the thin thickness of the nitrided layer. The irradiation of laser pulses onto a Ti target immersed in liquid N_2 is an interesting method for surface nitriding.

A similar synthesis experiment and the analysis were carried out by using a Si target. An X-ray diffraction (XRD) spectrum and the results of TEM analysis are shown in Fig. 9 [20]. As shown in

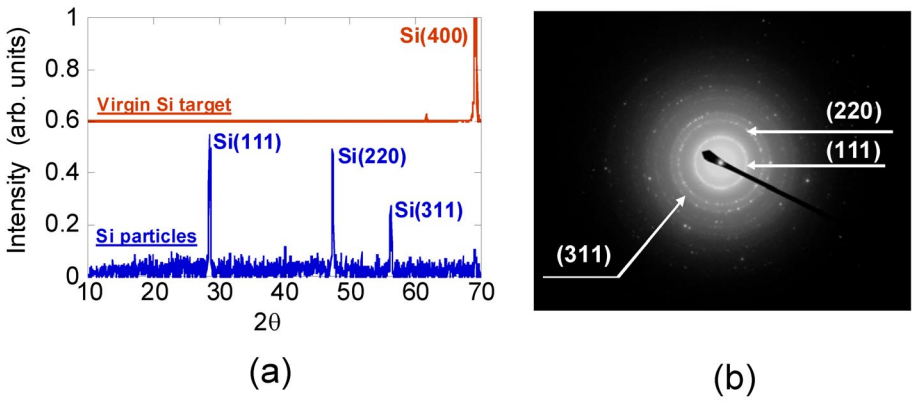

Fig. 9 (a) XRD spectrum and (b) electron diffraction pattern of nanoparticles produced by laser ablation of a Si target in liquid N_2.

Fig. 9a, we obtained nanoparticles of cubic Si having polycrystalline structure with (111), (220), and (311) orientations. The narrow widths of the peaks and the negligible broad background component in the XRD spectrum suggest high crystallinity. The electron diffraction pattern shown in Fig. 9b also indicates pure cubic Si nanoparticles with (111), (220), and (311) orientations. Laser ablation in liquid N_2 is a useful method for synthesizing crystalline pure Si particles with negligible oxidation.

CONTROL OF LIQUID-PHASE LASER ABLATION

There may be two concepts for the method of controlling liquid-phase laser-ablation: chemical and physical approaches. The chemical approach means using various liquid mediums (various organic solvents, solutions of various chemicals, etc.). We are currently investigating the control of liquid-phase laser ablation by using physical methods. A method we are trying is the control of the pressure and the temperature of water. For this experiment, we prepared a specially designed vessel which was compatible with a pressure up to 300 atm and a temperature of 500 °C. By increasing both the pressure and the temperature, we obtain supercritical water in the vessel and carry out laser ablation in supercritical water. In this paper, we show the control of the dynamics of the plasma and the cavitation bubble by changing the pressure of water.

Figure 10a shows the distributions of optical emission intensities along the perpendicular direction to the target surface observed when the pressures of water were 0.1 and 30 MPa [12]. The target was a Ti plate. As shown in Fig. 10a, we observed the compression of the plasma size by adding

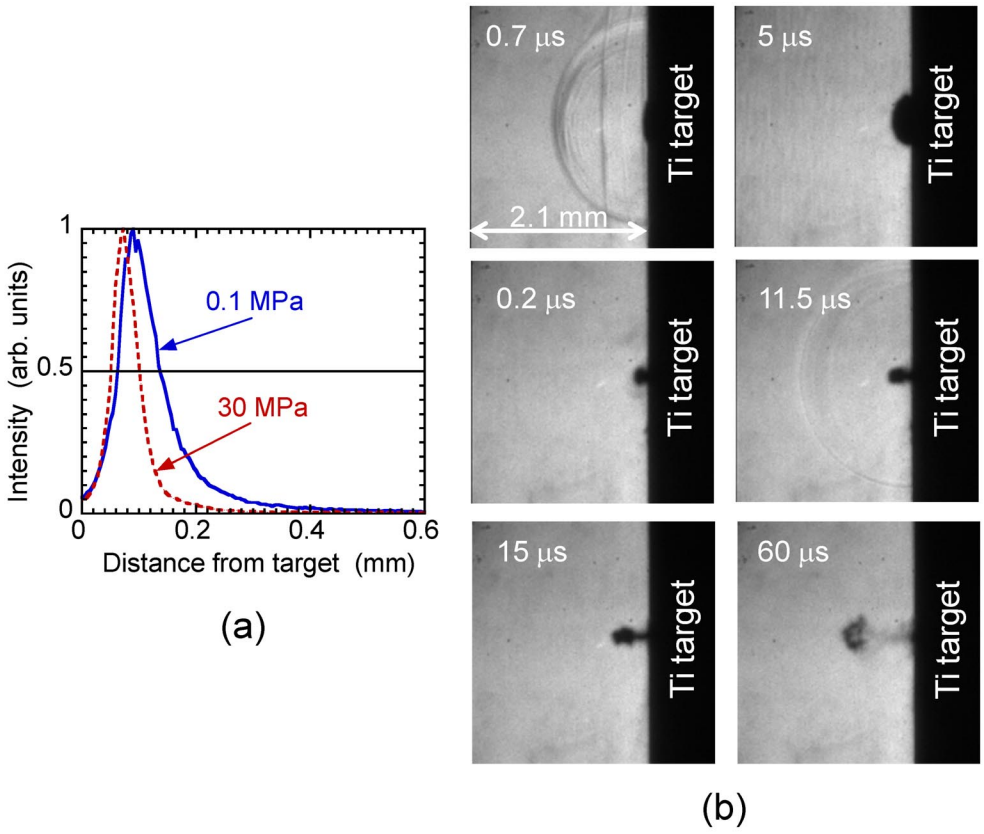

Fig. 10 (a) Distributions of optical emission intensities from laser-ablation Ti plasmas produced at 0.1 and 30 MPa. (b) Snapshots of cavitation bubbles induced by laser ablation of a Ti target in water at 3 MPa.

an external pressure of 30 MPa to water. The external pressure also affected the dynamics of the cavitation bubble. Figure 10b shows snapshots of shadowgraph imaging when we applied an external pressure of 3 MPa to water [14]. Comparing Fig. 10b with Fig. 4, the size of the cavitation bubble observed at 3 MPa was much smaller than that at 0.1 MPa. In addition, the collapse of the first cavitation bubble was observed at a much shorter delay time after laser ablation. A difference was also seen in the final shape of the cavitation bubble. In the case of 0.1 MPa, the final shape was a spherical bubble as shown in Fig. 4f, while in the case of 3 MPa, we observed the extinction of the cavitation bubble into water with a shape like a cloud as shown in Fig. 10b. These differences in the plasma and the cavitation bubble may affect the synthesis results of nanoparticles.

CONCLUSIONS

In this review article, we have shown that liquid-phase laser-ablation plasma has a high temperature of 10^4 K and a high pressure of 10^4 atm. Another high-temperature, high-pressure state is also realized at the collapse of a cavitation bubble. The laser light scattering experiment indicates the growth of nanoparticles inside the cavitation bubble. Interesting effects on the size and the structure of nanoparticles may be expected since they are in the high-temperature, high-density reaction field at the collapse of the cavitation bubble. As an example of applications, we have shown our unique experiment for synthesizing unoxidized nanoparticles by laser ablation in liquid N_2.

Although laser ablation is investigated mainly in the field of laser processing, it is strongly related to reactive plasmas. It is interesting that the interests in liquid-phase experiments are synchronized in both discharge and laser-ablation plasmas. In this paper, we emphasized the unusual features of laser-ablation plasmas which are never realized by discharges. However, we also believe that discharge and laser-ablation plasmas are complementary. We expect frequent communications between the research fields of discharge and laser-ablation plasmas.

ACKNOWLEDGMENTS

The authors are grateful to their students H. Ushida, T. Nakano, and W. Soliman for their contributions to this work. This work is supported partly by a Grant-in-Aid for Scientific Research on Innovative Areas “Frontier Science of Interactions between Plasmas and Nano-Interfaces” (No. 21110004) from the Ministry of Education, Culture, Sports, Science and Technology, Japan.

REFERENCES

1. O. Takai. *Pure Appl. Chem*. **80**, 2003 (2008).
2. F. Mafune, J. Kohno, Y. Takeda, T. Kondow, H. Sawabe. *J. Phys. Chem. B* **104**, 9111 (2000).
3. F. Mafune, J. Kohno, Y. Takeda, T. Kondow, H. Sawabe. *J. Phys. Chem. B* **105**, 5114 (2001).
4. C. H. Liang, Y. Shimizu, T. Sasaki, N. Koshizaki. *Appl. Phys. A* **80**, 819 (2005).
5. T. Tsuji, M. Watanabe, M. Tsuji. *Appl. Surf. Sci.* **211**, 189 (2003).
6. T. Sakka, K. Saito, Y. H. Ogata. *Appl. Surf. Sci.* **197–198**, 246 (2002).
7. Y. Yasui, H. Niino, Y. Kawaguchi, A. Yabe. *Appl. Surf. Sci.* **186**, 552 (2002).
8. G. W. Yang, J. B. Wang, Q. X. Liu. *J. Phys.: Condens. Matter* **10**, 7923 (1998).
9. P. Liu, Y. L. Cao, H. Cui, X. Y. Chen, G. W. Yang. *Chem. Mater.* **20**, 494 (2008).
10. X. Y. Chen, H. Cui, P. Liu, G. W. Yang. *Chem. Mater.* **20**, 2035 (2008).
11. H. Ushida, N. Takada, K. Sasaki. *J. Phys. Conf. Series* **59**, 563 (2007).
12. N. Takada, T. Nakano, K. Sasaki. *Appl. Surf. Sci.* **255**, 9572 (2009).
13. R. Fabbro, J. Fournier, P. Ballard, D. Devaux, J. Virmont. *J. Appl. Phys.* **68**, 775 (1990).
14. K. Sasaki, T. Nakano, W. Soliman, N. Takada. *Appl. Phys. Express* **2**, 046501 (2009).

15. T. Nakano, W. Soliman, N. Takada, K. Sasaki. *Technical Digest of 6th International Conference on Photo-Excited Processes and Applications*, p. 72, Sapporo, Japan (2008).
16. C. Brennen. *Cavitation and Bubble Dynamics*, Oxford University Press (1995).
17. W. Soliman, T. Nakano, N. Takada, K. Sasaki. *Technical Digest of 6th International Conference on Photo-Excited Processes and Applications*, p. 73, Sapporo, Japan (2008).
18. H. C. van de Hulst. *Light Scattering by Small Particles*, Dover, New York (1981).
19. W. Soliman, N. Takada, K. Sasaki. *Appl. Phys. Express* **3**, 035201 (2010).
20. N. Takada, T. Sasaki, K. Sasaki. *Appl. Phys. A* **93**, 833 (2008).
21. N. Takada, H. Ushida, K. Sasaki. *J. Phys. Conf. Series* **59**, 40 (2007).

